ISSN 0354-8724 (hard copy) | ISSN 1820-7138 (online)

Comparison of Daily and Monthly Intra-urban Thermal Reactions Based on LCZ Classification Using Surface and Air Temperature Data

Cathy Fricke[A*], Rita Pongrácz[B], János Unger[A]

Received: November 22, 2021 | Revised: January 10, 2022 | Accepted: January 12, 2022
doi: 10.5937/gp26-35050

Abstract

Urban air (T_a) and surface (T_s) temperature patterns depend mainly on the surface cover conditions. WUDAPT methodology was used to create the local climate zone (LCZ) map of Szeged (Hungary) providing detailed information about the structure of the urban area. The seasonal and monthly variations of simultaneous measurements of T_a (urban network) and T_s (MODIS) in different LCZs were analysed for a four-year period. The results show that the largest differences between T_s and T_a values occur in late spring and summer. During the day, the monthly mean T_s was much higher than the mean T_a, while at night, the T_a exceeded the T_s in all LCZs. Linear statistical relationship was also analysed, which concluded that diurnal and nocturnal T_a and T_s are strongly correlated in all LCZs in Szeged.

Keywords: urban heat island; air and surface temperatures; MODIS; urban network

Introduction

Rapid urbanization profoundly affected local climatic conditions, thus investigating the urban thermal environment gained importance in order to better adapt to changing conditions. The phenomenon known as the urban heat island (UHI) effect is a consequence of artificial surfaces and anthropogenic activities. UHI has an impact on the urban environment, including energy consumption, human health, phenological phases, duration of snow cover.

It is essential to distinguish between urban heat islands that are measured in the near-surface air layer (T_a, denoted by UHI) and those measured on the surface (T_s, denoted by SUHI) (Oke et al., 2017). Its magnitude is usually determined by urban heat island intensity, which by definition means an urban-rural temperature difference, although the demarcation between "urban" and "rural" areas is not clearly objective, making it very difficult to compare values reported in the scientific literature. For SUHI monitoring land cover products (Zhou et al., 2013) and night-time light data (Fu & Weng, 2018) are commonly used to distinguish and specify these areas.

Local Climate Zone (LCZ) scheme is a comprehensive classification system, its elements (zones) are 'regions of uniform surface cover, structure, material, and human activity that span hundreds of meters to several kilometers in horizontal scale' (Stewart & Oke, 2012). As this framework is able to represent the specific thermal regime of intra-urban areas, more and more studies appear that use the LCZ system in urban climate monitoring (e.g. Unger et al., 2011; Yang et al., 2018). The set of LCZs is divided into two sub-sets:

[A] Department of Climatology and Landscape Ecology, University of Szeged, Egyetem st. 2, H-6720 Szeged, Hungary; frcsaat@gmail.com; unger@geo.u-szeged.hu
[B] Department of Meteorology, Institute of Geography and Earth Sciences, ELTE Eötvös Loránd University, Pázmány Péter st. 1/A, H-1117, Budapest, Hungary, pongracz.rita@ttk.elte.hu
[*] Corresponding author: Cathy Fricke; e-mail: frcsaat@gmail.com

there are 10 built-up and 7 other land cover types, so they are very suitable for a fine and exact distinction between environments with urban and rural characteristics.

Several investigations (Bechtel & Daneke, 2012; Bechtel et al., 2015; Lelovics et al., 2014) focused on optimizing LCZ mapping methods and several studies followed them to develop and compare different classification procedures, considering local surface morphology (e.g. Geletič & Lehnert, 2016; Quan et al., 2017; Wang et al., 2018a; Hidalgo et al., 2019). These studies form four main groups: (i) GIS-based (Oliveira et al., 2020) and (ii) satellite-image-based classification, (iii) combined method, and (iv) expert-knowledge-based classification, as discussed in recent comprehensive review studies (Lehnert et al., 2021; Quan & Bansal, 2021).

Remote sensing imagery-based LCZ mapping supplies detailed urban morphology information for thermal characteristics analysis, and the usefulness was proved by a great amount of studies investigating LCZ–T_a relationship (e.g Yang et al., 2018). The mapping of LCZs expanded to many studies that focus on understanding the surface thermal characteristics. Some of them apply airborne measurements to assess the quality of LCZ classification, however it offers the opportunity for only short term detection (Skarbit et al., 2015; Bartesaghi Koc et al., 2018). Using thermal satellite images enabled to assess long-term and seasonal changes of the Ts in different LCZs (Gémes et al., 2016; Geletič et al., 2019), but their temporal resolution was low.

The World Urban Database and Portal Tool (WUDAPT 2021) was developed as an international synergy project to create a global high-resolution database that collects information on the urban form and function of cities worldwide using a universal, simple, and objective LCZ mapping method (Bechtel et al., 2015; Ching et al., 2014; See et al., 2015). Since then, this methodological framework has been successfully applied in mapping and thermal analysis studies. Bechtel et al. (2019a) conducted consistent and comprehensive inter-city SUHI analyses for 50 cities globally from MODIS (Moderate Resolution Imaging Spectroradiometer) and Landsat data. Significant Ts differences were detected within the built-up classes, confirming the suitability of the LCZ system and WUDAPT L0 data for SUHI analysis. However, considerable differences were found in the spatial distribution of SUHIs between cities, which can be explained by phenology, topography, and the influence of neighbouring LCZ classes.

Many other studies confirmed the strong LCZ–T_s relationship in urban regions in wet subtropical areas (Das & Das, 2020) as well as in arid areas (Wang et al., 2018b; Fricke et al., 2020) using WUDAPT methodology. Dian et al. (2020) applied remote sensing data to examine the spatial and temporal structures of T_s, and they concluded that the differentiation of LCZs by T_s depends on the time of the day in the case of Budapest. Du et al. (2020) combined LiDAR and satellite data to study the thermal behaviors of different LCZs and their results show that in Nanjing the thermal reactions of LCZs were more distinguishable by T_s in summer than in other seasons, and building height had a substantial effect on T_s.

Gholami & Beck (2019) revealed a significant relationship between LCZ and T_s on the basis of case studies from 25 cities worldwide with different climatic backgrounds. They investigated the influential drivers of the relationship when applying the WUDAPT concept, and their results demonstrated that latitude, mean and maximum annual temperature were the dominant modifier factors among the examined possible factors.

Another group of research (Beck et al., 2018; Oxoli et al., 2018) focused on the relationship between LCZ classes and air temperature. The analysis by Skarbit et al. (2017) aimed at comparing T_a in different LCZ classes, and their results show that the temperature parameters of compact LCZs exceed those of the other classes. Besides in-situ observations, T_a difference was examined also via mobil measurements (Stewart et al., 2014; Leconte et al., 2015) and high correlation was detected between LCZs and T_a.

In order to better understand the urban thermal environment, some articles aimed at combining T_s and T_a observations, and in parallel, compared the spatial and temporal variability of T_a and T_s, and sought to explore their relationship. Gallo & Owen (1999) investigated the relationship of urban-rural T_a–T_s–NDVI differences and they concluded that T_s is a useful predictor of monthly and seasonal T_a variables for the period from March to June. Yang et al. (2020) quantified UHI/SUHI difference simultaneously with five different indicators in Changchun (China), where light snows occur in winter. According to the results the land cover of the demarcated "urban" and "rural" areas has a substantial influence on UHI/SUHI intensity. Li et al. (2020) analysed the relationship between SUHI and T_a, and their results indicate that T_a has a spatially nonstacionary impact on SUHI.

However, it can be concluded that little effort has been made to investigate the complex relationship between LCZ–T_s–T_a using a large number of thermal remote sensing datasets, allowing detailed daily and monthly analysis of variation.

In this study, we focus on the analysis of thermal reactions between LCZs and the rural areas as well, as within the city using the example of a Central Euro-

pean city (Szeged, Hungary) based on 4-years (2014–2018) of simultaneous satellite and urban station network data sets. Our specific objectives are to:

1. collect MODIS thermal images with clear conditions and separate them according to months as well, as night and day;
2. collect simultaneous air temperature data from the urban station network of Szeged and separate them according to months as well, as night and day;
3. compare the obtained mean monthly (seasonal) diurnal and nocturnal Ts and Ta differences between the urban LCZs and rural areas.

Study area

Szeged (46.25°N, 20.15°E) with a population of 160,000 is the third largest city in Hungary locating on the Great Hungarian Plain (Figure 1a). Szeged is characterised by densely populated urban area with a concentric growth pattern and fragmented suburban areas (Figure. 1b). The core of the city is characterised by midrise buildings, and it is surrounded by warehouses, detached houses with gardens, and blocks of flats in the north-eastern direction. Its neighbouring rural area is utilized for cultivating different crops, but a few groups of trees are also found there. Its climate is Cfa by the climate classification of Köppen (1918) with the highest monthly temperature of 22.7 °C and the annual amount of precipitation of 508 mm (1986–2015, Harris et al., 2014).

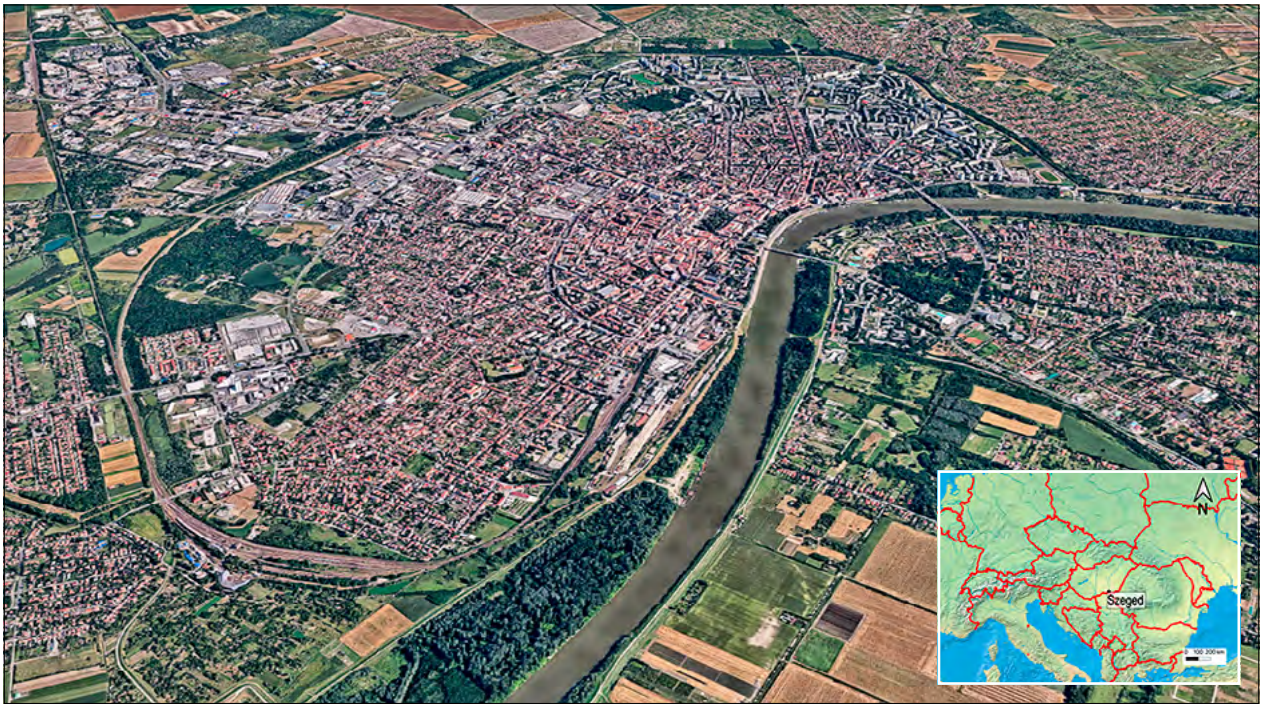

Figure 1. The geographical location of Szeged in Hungary and Europe, and its aerial view (https://www.google.com/maps)

Data and methods

LCZ mapping and separating urban and rural areas

The applied mapping method uses freely accessible software (Google Earth and SAGA-GIS) and remotely sensed data (Bechtel et al., 2015), and it provides a globally objective classification (Bechtel et al., 2019b). The first step of the workflow is processing all the 11 spectral bands of Landsat-8 satellite images. The highest quality level Precision Terrain dataset of the Operational Land Imager and the Thermal Infrared Sensor instruments was downloaded from the Earth Explorer user interface of the U.S. Geological Survey (https://earthexplorer.usgs.gov). In order to represent the intra-annual surface changes, cloud-free Landsat-8 images were taken at three different times of the year, namely, on 24.06.2017, 27.08.2017 and 30.10.2017. Secondly, we need to resample the 30–100 m resolution Landsat-8 scenes to a common spatial resolution (100 m) in SAGA-GIS. The next part of the process is to delineate manually the training area polygons of the LCZ classes and the region of interest in Google Earth.

In SAGA-GIS an automated classification of Landsat images was conducted using random forest classification algorithm. If poorly classified areas are detected, we have to improve the training areas, and repeat the classification procedure as many times as necessary. In a final step, a majority post-filtering is performed with a given filter radius size to scan the neighbouring pixels around a central pixel. After testing different radius sizes, we selected 3 pixels in the current study, because this reduces noise, but meanwhile, it does not result in unreasonable generalisation at this city scale. The result of this workflow is an LCZ map of the study area (for more details see Fricke et al. (2020)).

Figure 2 shows the obtained LCZ map for Szeged. Seven different built-up LCZs were distinguished: 2 (compact mid-rise), 3 (compact low-rise), 5 (open mid-rise), 6 (open low-rise), 8 (large low-rise), 9 (sparsely built), and 10 (heavy industry). As it can be seen the built-up density is decreasing beginning from the downtown to the border of the city. The northwestern part of the city covered by LCZ 8 and LCZ 10 is located beyond the urban area (see later).

Around the city 5 different land cover types were detected: LCZ A (dense trees), LCZ B (scattered trees), LCZ C (bush, scrub), LCZ D (low plants), and LCZ G (water). The dominant land cover type of the surrounding area is LCZ D with low plants (Figure 2).

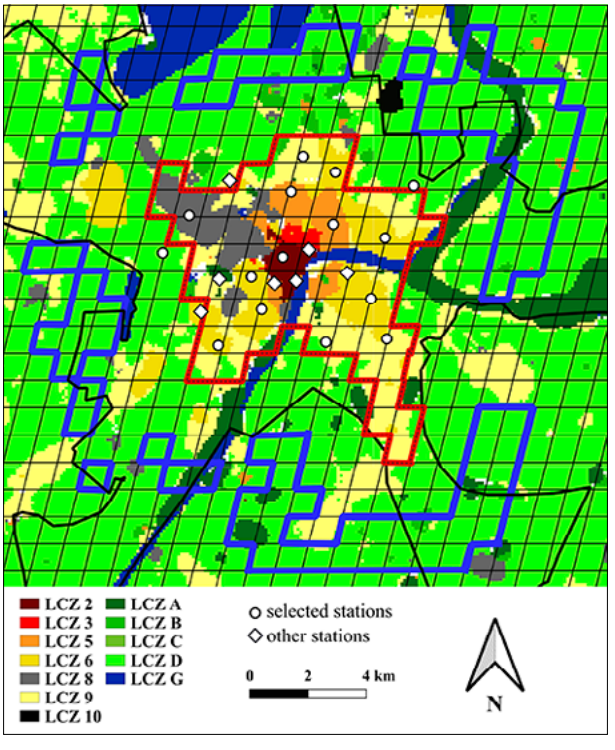

Figure 2. LCZ map shown on the MODIS grid covering the study area with administrative city border (black line), delineated urban (red line) and rural (blue line) polygons in and around Szeged (the elements of the 24-station network are marked by circles and squares)

Some parts of the low plant areas are under agricultural use, which means that they became bare soil temporarily within the year, thus bare soil and low plant areas are merged into LCZ D. As we used multiple satellite images from different dates, the merging of the two zones simplifies the classification.

To make a comprehensive study we identified urban and rural areas using the obtained LCZ map. In QGIS we assessed the ratios of individual LCZ classes for each MODIS tile. Urban and rural tiles are determined by different criteria which are specified in Fricke et al. (2020). We considered tiles as urban tiles if they are covered by mostly built-up LCZs and during selection of rural area we eliminated significant effects of built-up areas, water bodies or substantial topography (Table 1).

Table 1. Specification of urban and rural tiles

Urban	Rural
• include min. 55% built-up LCZs • cells form coherent area • located within the administrative border	• mostly uninhabited • located at least 2 km from the urban boundary • must contain less than 1% of total building surface fraction

Source: Fricke et al., 2020

Land surface (T_s) and air (T_a) temperature

In this paper MOD11A1 (V6) MODIS/Terra and MYD11A1 (V6) MODIS/Aqua Land Surface Temperature and Emissivity Daily L3 Global 1 km Grid SIN products were used to investigate surface thermal properties. Data were obtained from the summer of 2014 to the spring of 2018 for the study area. Sensor MODIS measurements are available from both solar-synchronous satellites Terra and Aqua as part of the American National Aeronautics and Space Administration's Earth Observing System. The MODIS sensor measures radiation in 36 electromagnetic spectral bands with different spatial resolutions (NASA, 1999). T_s retrieved from the raw MODIS radiation data by split window algorithm, which corrects the atmospheric effects using multiple bands on the sensor MODIS (Wan & Snyder, 1999). This method is less sensitive to uncertainty in emissivity over wide ranges of surface and atmospheric conditions resulting in improved data quality.

Both Terra and Aqua images consisted of one day- and one nighttime scenes with acquisition times approximately 9–10 a.m., 8–9 p.m. (Terra), 2–3 a.m. and 12–13 p.m. (Aqua). Since anticyclonic, cloudless weather situations enable us to examine the local-scale thermal patterns, only the images that contained 100% data coverage within the delineated urban and rural areas ofSzeged.

The air temperature (T_a) data came from the urban monitoring network of Szeged, similar to the one in Novi Sad, Serbia (Šećerov et al., 2019). It was established to provide long-term T_a and relative humidity datasets from various parts of the city representing different local environments. The selection and installation of 24 station sites considered the spatial pattern of the LCZs in order to gain representative temperature datasets for these zones (see Figure. 2). 22 stations settled in the urban area of the city, while stations D-1 and D-2 are situated in its rural surroundings (for more details see Skarbit et al. (2017)).

We selected those T_a stations as urban stations, which are located in MODIS cells with more than 55% coverage by a particular built-up LCZ class and we considered D-1 and D-2 stations as representatives of the rural area. The selection provided one station in LCZ 2, two stations in LCZ 5, six stations in LCZ 6, one station in LCZ 8, and three stations in LCZ 9 within the urban area (Figure 2).

Calculation, evaluation and comparison of daily and monthly variation of T_s and T_a

From the measurements of the selected stations, the hourly means of T_a were retrieved for the acquisition times of sensor MODIS. Those stations were selected where the built-up LCZ coverage exceeded 50% in a MODIS pixel. Missing data were filtered out and only the simultaneous measurements of a particular MODIS pixel and its inherent T_a station were taken into account during the further computations. For LCZs (5, 6 and 9) with more than one station, the collected data were averaged. The T_s and T_a data were separated into diurnal and nocturnal groups on the basis of the forenoon/afternoon and night/dawn MODIS images, and the simultaneous T_a data, respectively.

As the first step, we calculated the monthly mean diurnal and nocturnal T_s and T_a differences between urban LCZs and rural areas ($\Delta T_{s(LCZx\text{-}r)}$) and $\Delta T_{a(LCZx\text{-}r)}$, respectively). Then, these mean diurnal and nocturnal values were compared for each month, and the retrieved differences of the thermal reactions of surface and air by LCZs were analysed and explained (see later Figures 3 and 4).

As the second step, the annual variations of T_s and T_a were demonstrated on box plots for LCZ 2 and LCZ D as they respresent the most different (densely built up and rural) land cover (see later Figure 5).

As the third step, linear statistical relationships between all available T_s and T_a values were revealed and evaluated by LCZs (see later Figure 6).

Results and discussion

In this section several analyses were undertaken to reveal the relationship between the different thermal characteristics as well as between these thermal characteristics and LCZ classes.

Comparison of daily and monthly intra-urban thermal reactions

Figure 3 shows the annual variation of diurnal and nocturnal thermal differences measured in surface temperatures between different urban LCZs and the surrounding rural area of Szeged. Figure 4 presents the annual variation of the T_s–T_a differences by LCZs both in daytime and nighttime.

It can be immediately seen in Figure 4, that during the day T_s was much higher than T_a (especially in the warm half-year). At night, the opposite was detected in all zones, with the air being warmer than the surface, although not to the same extent as during daytime. No substantial T_a difference was observed between urban LCZs and rural areas in daytime (Figure 3a). Urban LCZs are mostly cooler by around 1 °C, and the differences are almost constant throughout the year, with a few exceptions (e.g., LCZ 8 in February, LCZ 6 in April).

The largest T_s difference (4.1 °C) was observed between LCZ 2 and the rural area during daytime in June (Figure 3b). While the Ts difference between LCZ 2 and rural area changed by the seasonal variation of the solar irradiation, a relatively slight seasonal variation was observed in T_s in other zones. In September and October, the largest $\Delta T_{s(LCZx\text{-}r)}$ was observed in LCZ 8, which is mostly dominated by large shopping centers and industrial buildings. From late autumn to late winter, there was no considerable Ts-difference between individual LCZs, presumably due to the more insignificant vegetation typical for this period (Figure 3b).

The highest T_s–T_a difference (9.7 °C) was found in LCZ 2 during daytime in May, and T_s was more than 7 °C higher compared to T_a from April to August, while the lowest T_s–T_a difference was observed for LCZ D and LCZ 9, which consist mostly of green areas (Figure 4).

At night, $\Delta T_{a(LCZx\text{-}r)}$ is consistent with the built-up density: the difference increases with building density, so that the largest difference occurs almost throughout the year between LCZ 2 and the rural area (Figure 3c). LCZs 5 and 8 are the second warmest zones followed by the LCZs 6 and 9. The seasonal variation of the nocturnal $\Delta T_{a(LCZx\text{-}r)}$ is relatively large compared to the daytime situation (Figure 3a).

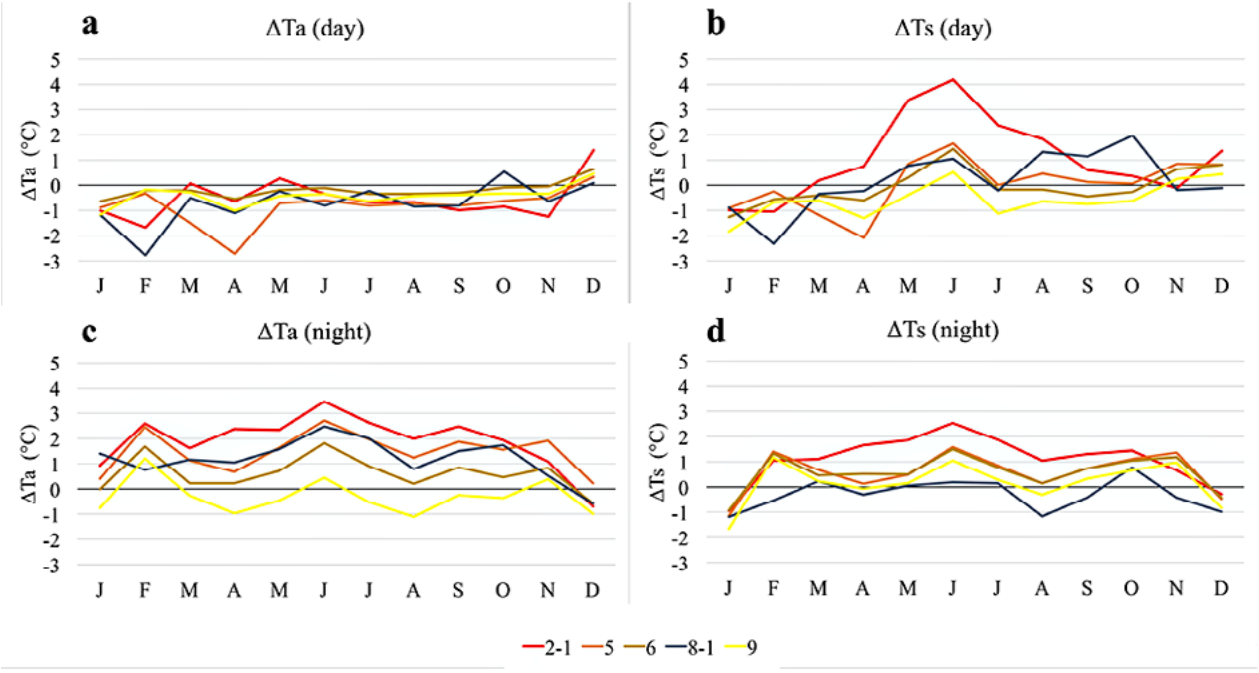

Figure 3. Annual variation of the diurnal (a, b) and nocturnal (c, d) LCZ vs. rural thermal differences detected in surface ($\Delta T_{s(LCZx-r)}$) and air ($\Delta T_{a(LCZx-r)}$) temperatures (Szeged, clear days, 01.06.2014 – 31.05.2018)

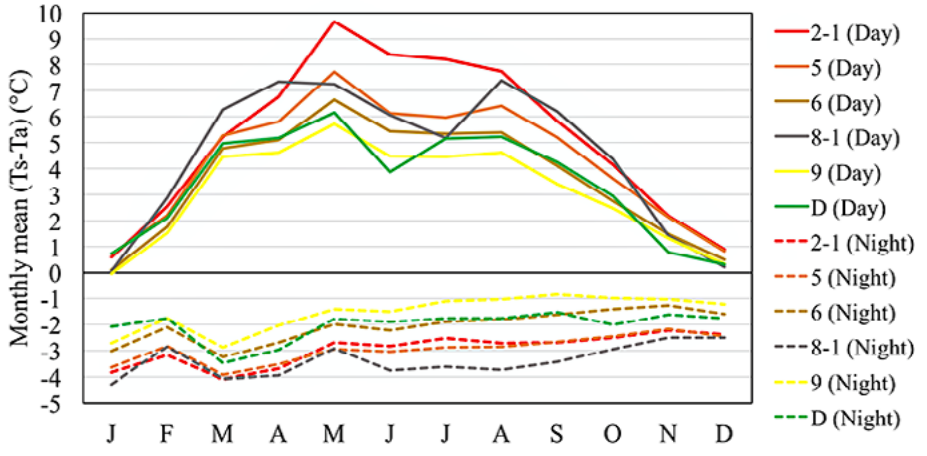

Figure 4. Annual variation of the diurnal and nocturnal T_s–T_a differences by LCZs (Szeged, clear days, 01.06.2014 – 31.05.2018)

Regarding the nocturnal dynamics of $\Delta T_{s(LCZx-r)}$, there were only small differences between the LCZ classes (Figure 3d). From February to October, the LCZ 2 was at least 1 °C warmer than the rural area, however, the difference exceeded 2 °C also in June.

Seasonal thermal reactions of LCZ D and LCZ 2

The thermal effects of the built-up differences were investigated among the LCZs having the most diverse surface properties (LCZs D and 2), comparing the obtained seasonal T_a and T_s values. In Figure 5, the boxplots of these LCZs show the median values of the measured and seasonally averaged absolute T_s and T_a values as well, as their distribution (showing quartiles and extremes) and outliers (indicated by open circles). It can be clearly seen that during the day, the absolute T_a and T_s values increase with seasonally increasing insolation for both LCZ 2 and LCZ D. In addition, the T_s values are mostly higher than the T_a values during daytime, while the T_a exceeds the T_s at night, regardless of the season.

The diurnal T_a and T_s values show greater variability in spring and autumn than in other seasons as the thin vertical lines between the extremes cover relatively broader intervals (Figure 5). Most outliers were observed in winter in both LCZs, however, the two LCZs' thermal reactions were less distinguishable then. The LCZ D and LCZ 2 are well distinguished during daytime in summer: the T_s values vary between 24.5–44.5 °C and 26.6–46.5 °C in LCZ D and in LCZ 2, respectively.

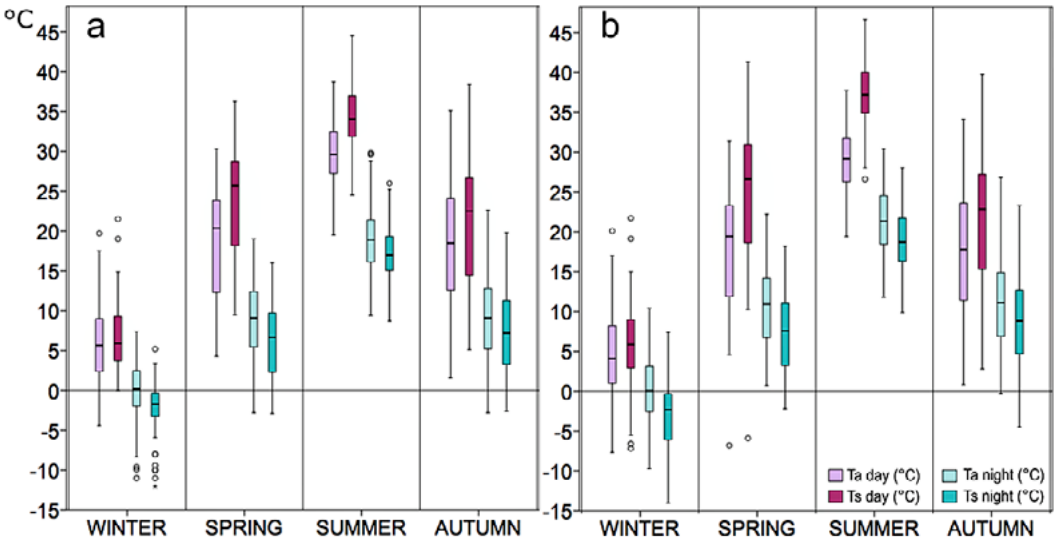

Figure 5. Annual variation of the diurnal and nocturnal thermal reactions of (a) LCZ D and (b) LCZ 2 detected in surface (T_s) and air (T_a) temperatures, as examples (Szeged, clear days, 01.06.2014 – 31.05.2018)

Linear statistical relationships between surface and air temperatures

Figure 6 shows the scatter plots of the correlation between the parallel T_s and T_a records of MODIS and urban stations in each LCZ during day and night. According to these, strong linear relationship can be detected in each LCZ both day and night in the study area. LCZ 5 (Figure 6b), LCZ 6 (Figure 6c) and LCZ 9 (Figure 6e) contain more than one station, which obviously results in more observation pairs than LCZ 2 (Figure 6a), LCZ 8 (Figure 6d) and LCZ D (Figure 6f). The coefficients of determination (R^2) were very high, ranging from 0.92 (LCZ D) to 0.982 (LCZ 5) during daytime, and slightly lower at night, between 0.912 (LCZ 9) and 0.959 (LCZ 2).

Hereher and El Kenawy (2020) also reported strong correlations between the monthly daily and nocturnal T_s and the minimum as well, as maximum T_a values. Similar results were also concluded in many other studies (e.g. Zhu et al., 2013; Chen et al., 2016). The derivation of the diurnal linear regression changed around 0.8, while the nocturnal derivation was above 0.9. The diurnal T_s is generally higher than diurnal T_a, while T_a and T_s values are quite close at night.

Conclusions

This study classified LCZs in and around Szeged using Landsat 8 satellite images based on the WUDAPT method. As a result, 7 different built-up LCZs were recognised in the urban area of Szeged. T_a values are retrieved from the urban monitoring network of Szeged, while the T_s database was provided by MODIS.

Simultaneously measured T_s and T_a values were compared in each MODIS pixel that contained at least one T_a station and had more than 50% coverage of a built-up LCZ. Seasonal and monthly variations in thermal differences in the built-up LCZs were analyzed, and T_s values were generally higher during the day, especially in summer, while T_a at night mostly exceeded T_s in all LCZs. The nocturnal LCZ–rural differences of T_a increased with increasing built-up density, while T_s showed the same pattern, both during day and night. Over the four-year period studied, the highest mean T_s difference (4.1 °C) ***was observed*** between LCZ 2 and the rural area, during daytime in June. Seasonal variation of thermal properties were investigated between LCZ 2 and LCZ D as these LCZs represent the most densely built-up urban and the most dominantly present rural LCZs, respectively. The results show a high thermal contrast, especially in summer and spring during the daytime period. Analysis of the T_s–T_a correlation showed that a strong linear relationship was observed in all LCZs day and night.

Results show that built-up density and the amount of vegetation has a considerable effect on the thermal pattern of the urban and the surrounding areas. Adding more vegetation, replacing artificial surface to natural would decrease local and microscale differences. In addition prefering lower built-up density in urban planning would also mitigate urban heat island effect. Expected increasing global temperature and heat waves associated with climate change will enhance this urban-rural contrast, which has also negative impacts on human thermal comfort and energy

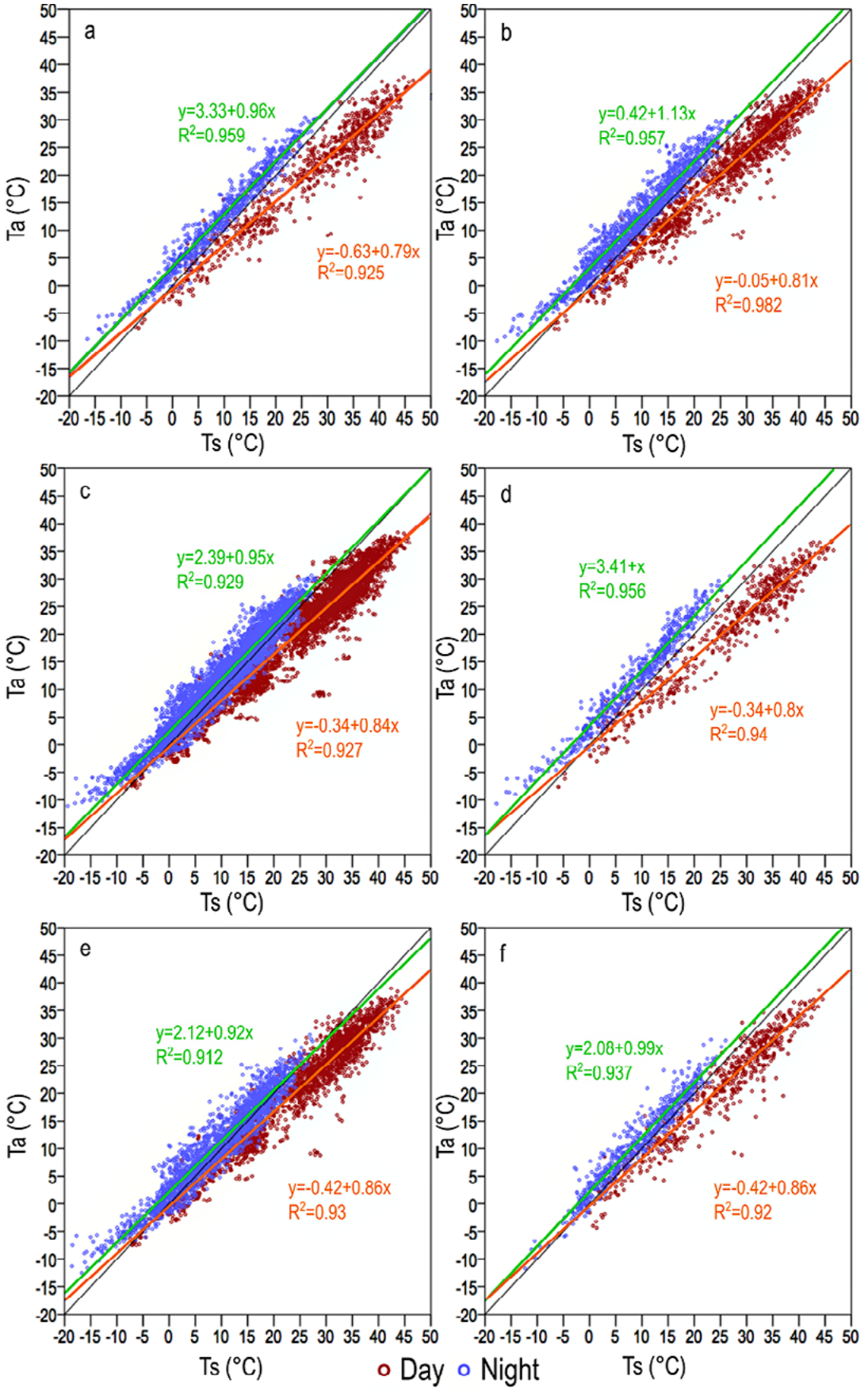

Figure 6. Linear regression relationship (orange lines: day, green lines: night) fitted between surface (T_s) and air (T_a) temperatures by LCZs (a – LCZ 2, b – LCZ 5, c – LCZ 6, d – LCZ 8, e – LCZ 9, f – LCZ D) (Szeged, clear days, 01.06.2014 – 31.05.2018)

consumption. Increasing temperatures will become more intolerable for urban inhabitants in the densely built-up regions of the cities, while people who live in areas of openly arranged buildings will experience less heat excess. For this reason preffering open city structure during urban planning and improving resilient infrastructures by local government would mitigate these disadvantageous effects and it would help in adaptions to ongoing climate change.

This paper was the first step of our extended research on T_s-T_a relationship therefore we examined it only one urban area (Szeged). In the future our aim is to accomplish a larger scale investigation with more cities in Central Europe to find different relationships between the studied thermal variables using statistical models which would enable us to assess the UHI effect also in cities where urban monitoring network is not available.

Acknowledgements

MODIS data were retrieved from the Data Pool (https://lpdaac.usgs.gov/data_access/data_pool). Landsat data were retrieved from www.earthexplorer.usgs.com. The research has been supported by the National Research, Development and Innovation Office, Hungary (K-129162, K-137801).

References

Barteshagi K. C., Osmond, P., Peters, A. & Irger, M. (2018). Understanding land surface temperature differences of Local Climate Zones based on airborne remote sensing data. IEEE *Journal of Selected Topics in Applied Earth Observation and Remote Sensing,* 11, 2724–2730. https://doi.org/10.1109/JSTARS.2018.2815004

Bechtel, B. & Daneke, C. (2012). Classification of Local Climate Zones based on Multiple Earth observation data. *IEEE Journal of Selected Topics in Applied Earth Observations and Remote Sensing,* 99, 1–5. https://doi.org/10.1109/JSTARS.2012.2189873

Bechtel, B., Alexander, P.J., Böhner, J., Ching, J., Conrad, O., Feddema, J., Mills, G., See, L. & Stewart, I. (2015). Mapping Local Climate Zones for a Worldwide Database of the Form and Function of Cities. *ISPRS Internation Journal of Geo-Information,* 4, 199–219. https://doi.org/10.3390/ijgi4010199

Bechtel B., Demuzere, M., Mills, G., Zhan, W., Sismanidis, P., Small, C. & Voogt, J. (2019a). SUHI analysis using Local Climate Zones—A comparison of 50 cities. *Urban Climate*, 28, 100451. https://doi.org/10.1016/j.uclim.2019.01.005

Bechtel, B., Alexander, P., Beck, C., Böhner, J., Brousse, O., Ching, J., Demuzere, M., Fonte, C., Gál, T., Hidalgo, J., Hoffmann, P., Middel, A., Mills, G., Ren, C., See, L., Sismanidis, P., Verdonck, M. L., Xu, G. & Xu, Y. (2019b). Generating WUDAPT Level 0 data – Current status of production and evaluation. *Urban Climate*, 27, 24–45. https://doi.org/10.1016/j.uclim.2018.10.001

Beck, C., Straub, A., Breitner, S., Cyrys, J., Philipp, A., Rathmann, J., Schneider, A., Wolf, K. & Jacobeit, J. (2018). Air temperature characteristics of local climate zones in the Augsburg urban area (Bavaria, southern Germany) under varying synoptic conditions. *Urban Climate*, 25, 152–166. https://doi.org/10.1016/j.uclim.2018.04.007

Chen, Y., Sun, H. & Li, J. (2016). Estimating daily maximum air temperature with MODIS data and a daytime temperature variation model in Beijing urban area. *Remote Sensing Letters*, 7(9), 865–874. https://doi.org/10.1080/2150704X.2016.1193792

Ching, J., See, L., Mills, G., Alexander, P., Bechtel, B., Feddema, J., Oleson, K.L., Stewart, I., Neophytou, M., Chen, F., Wang, X. & Hanna A. (2014). WUDAPT: Facilitating advanced urban canopy modeling for weather, climate and air quality applications. In: 94th American Meterological Society Annual Meeting, 2-6 February 2014, Georgia, USA.

Clinton, N. & Gong, P. (2013). MODIS detected surface urban heat islands and sinks: global locations and controls. *Remote Sensing of Environment,* 134, 294–304. https://doi.org/10.1016/j.rse.2013.03.008

Das, M. & Das, A. (2020). Assesing the relationship between local climate zones (LCZs) and land surface temperature (LST) – A case study of Sriniketan-Santiniketan Planning Area (SSPA), West Bengal, India. *Urban Climate*, 32, 1–18. https://doi.org/10.1016/j.uclim.2020.100591

Dian, Cs., Pongrácz, R., Dezső, Zs. & Bartholy, J. (2020). Annual and monthly analysis of surface urban heat island intensity with respect to the local climate zones in Budapest. *Urban Climate*, 31, 100573. https://doi.org/10.1016/j.uclim.2019.100573

Du, P., Chen, J., Bai, X. & Han, W. (2020). Understanding the seasonal variations of land surface temperature in Nanjing urban area based on local climate zone. *Urban Climate*, 33, 100657. https://doi.org/10.1016/j.uclim.2020.100657

Fricke, C., Pongrácz, R., Gál, T., Savic, S. & Unger, J. (2020). Using local climate zones to compare remotely sensed surface temperatures in temperate cities and hot desert cities. *Moravian Geographical Reports,* 28, 48–60. https://doi.org/10.2478/mgr-2020-0004

Fu, P. & Weng, Q. (2018). Variability in annual temperature cycle in the urban areas of the United States as revealed by MODIS imagery. *ISPRS Journal of Photogrammetry and Remote Sensing*, 146, 65–73. https://doi.org/10.1016/j.isprsjprs.2018.09.003

Geletič, J. & Lehnert, M. (2016). A GIS-based delineation of local climate zones: The case of medium-sized Central European cities. *Moravian Geographical Reports*, 24(3), 2–12. https://doi.org/10.1515/mgr-2016-0012

Geletič, J., Lehnert, M. & Dobrovolný, P. (2016). Land surface temperature differences within Local Climate Zones, based on two Central European cities. *Remote Sensing,* 8. https://doi.org/10.3390/rs8100788

Geletič, J., Lehnert, M., Savić, S. & Milošević, D. (2019). Inter-/intra-zonal seasonal variability of the surface urban heat island based on local climate zones in three central European cities. *Building and Environment,* 156, 21–32. https://doi.org/10.1016/j.buildenv.2019.04.011

Gallo, K.P. & Owen, T.W. (1999). Satellite-based adjustments for the urban heat island temperature bias. *Journal of Applied Meteorology*, 38(6), 806–813. https://doi.org/10.1175/1520-0450(1999)038<0806:SBAFTU>2.0.CO;2

Gholami, R.M. & Beck, C. (2019). Towards the determination of driving factors of varying LST-LCZ relationship: A case study over 25 cities. *Geographica Pannonica*, 23, 289–307. https://doi.org/10.5937/gp23-24238

Harris, I., Jones, P.D., Osborn, T.J. & Lister, D.H. (2014). Updated high-resolution grids of monthly climatic observations – the CRU TS3.10 Dataset. *International Journal of Climatology*, 34, 623–642. https://doi.org/10.1002/joc.3711

Hereher, M.E. & El Kenawy, A. (2020). Extrapolation of daily air temperatures of Egypt from MODIS LST data. *Geocarto International*, 1-17. https://doi.org/10.1080/10106049.2020.1713229

Hidalgo, J., Dumas, G., Masson, V., Petit, G., Bechtel, B., Bocher, E., Foley, M., Schoetter, R. & Mills, G. (2019). Comparison between local climate zones maps derived from administrative datasets and satellite observations. *Urban Climate*, 27, 64–89. https://doi.org/10.1016/j.uclim.2018.10.004

Köppen, W. (1918). Klassifikation der Klimate nach Temperatur, Niederschlag und Jahreslauf. Classification of climates according to temperature, precipitation and the course oft he year. *Pettersman Geographische Mitteilungen*, September/Oktoberheft, 193–203.

Leconte, F., Bouyer, J., Claverie, R. & Pétrissans, M. (2015). Using Local Climate Zone scheme for UHI assessment: Evaluation of the method using mobile measurements. *Building and Environment,* 83, 39–49. https://doi.org/10.1016/j.buildenv.2014.05.005

Lehnert, M., Savić, S., Milošević, D., Dunjić, J. & Geletič, J. (2021). Mapping Local Climate Zones and their applications in European urban environments: A systematic literature review and future development trends. *ISPRS International Journal of Geo-Information*, 10, 260. https://doi.org/10.3390/ijgi10040260

Lelovics, E., Unger, J., Gál, T. & Gál, C.V. (2014). Design of an urban monitoring network based on Local Climate Zone mapping and temperature pattern modelling. *Climate Research*, 60, 51–62. https://doi.org/10.3354/cr01220

Li, L., Zha, Y. & Wang, R. (2020). Relationship of surface urban heat island with air temperature and precipitation in global large cities, *Ecological Indicators*, 117, 106683. https://doi.org/10.1016/j.ecolind.2020.106683

National Aeronautics and Space Administration, (1999). Science writers' guide to Terra. NASA Earth Observing System Project Science Office, Greenbelt, MD. 28p.

Oke, T.R., Mills, G., Christen, A. & Voogt, J.A. (2017). *Urban Climates*. Cambridge, Cambridge University Press.

Oliveira, A., Lopes, A. & Niza, S. (2020). Local climate zones in five southern European cities: An improved GIS-based classification method based on Copernicus data. *Urban Climate*, 33, 100631. https://doi.org/10.1016/j.uclim.2020.100631

Oxoli, D., Ronchetti, G., Minghini, M., Molinari, M.E., Lotfian, M., Sona, G. & Brovelli, M.A. (2018). Measuring urban land cover influence on air temperature through multiple Geo-Data—The case of Milan, Italy. *ISPRS International Journal of Geo-Information*, 7, 421. https://doi.org/:10.3390/ijgi7110421

Quan, J.Q. & Bansal, P. (2021). A systematic review of GIS-based local climate zone mapping studies. *Building and Environment,* 196, 107791. https://doi.org/10.1016/j.buildenv.2021.107791

Quan, S. J., Dutt, F., Woodworth, E., Yamagata, Y. & Yang, P.P-J. (2017). Local Climate Zone mapping for energy resilience: A fine-grained and 3D approach. *Energy Procedia*, 105, 3777–3783. https://doi.org/10.1016/j.egypro.2017.03.883

See, L., Perger, C., Dürauer, M., Fritz, S., Bechtel, B., Ching, J., Alexander, P., Mills, G., Foley, M., O'Connor, M., Stewart, I., Feddema, J. & Masson V.

(2015). Developing a community-based worldwide urban morphology and materials database (WUDAPT) using remote sensing and crowdsourcing for improved urban climate modelling. Joint Urban Remote Sensing Event (JURSE 2015) Lausanne. 208–211.

Šećerov, I., Savić, S., Milošević, D., Arsenović, D., Dolinaj, D. & Popov, S. (2019). Progressing urban climate research using a high-density monitoring network system. *Environmental Monitoring and Assessment,* 191. https://doi.org/10.1007/s10661-019-7210-0

Skarbit, N., Gál, T. & Unger, J. (2015). Airborne surface temperature differences of the different Local Climate Zones in the urban area of a medium sized city. Joint Urban Remote Sensing Event (JURSE 2015), Lausanne, Switzerland, PID3445901. https://doi.org/10.1109/JURSE.2015.7120497

Skarbit, N., Stewart, I.D., Unger, J. & Gál, T. (2017). Employing an urban meteorological network to monitor air temperature conditions in the 'local climate zones' of Szeged, Hungary. *International. Journal of Climatology*, 37(S1), 582–596. https://doi.org/10.1002/joc.5023

Stewart, I.D. & Oke, T.R. (2012). Local Climate Zones for urban temperature studies. *Bulletin of the. American Meteorological Society,* 93, 1879–1900. https://doi.org/10.1175/BAMS-D-11-00019.1

Stewart, I.D., Oke, T.R. & Krayenhoff, E.S. (2014). Evaluation of the 'local climate zone' scheme using temperature observations and model simulations. *International Journal of Climatology*, 34, 1062–1080. https://doi.org/10.1002/joc.3746

Unger, J., Savić, S. & Gál, T. (2011). Modelling of the annual mean urban heat island pattern for planning of representative urban climate station network. *Advances in Meteorology*, 398613. https://doi.org/10.1155/2011/398613

U.S. Geological Survey. Available at: https://earthexplorer.usgs.gov (last accessed: 15 March 2021)

Wan, Z. & Snyder, W. (1999). MODIS land-surface temperature algorithm theoretical basis document. Institute for Computational Earth Systems Science, University of California, Santa Barbara.

Wang, R., Ren, C., Xu, Y., Lau, K.K-L. & Shi, Y. (2018a). Mapping the local climate zones of urban areas by GIS-based and WUDAPT methods: A case study of Hong Kong. *Urban Climate*, 24, 567–575. https://doi.org/10.1016/j.uclim.2017.10.001

Wang, C., Middel, A., Myint, S.W., Kaplan, S., Brazel, A.J. & Lukasczyk, J. (2018b). Assessing local climate zones in arid cities: The case of Phoenix, Arizona and Las Vegas, Nevada. *ISPRS Journal of Photogrammetry and Remote Sensing*, 141, 59–71. https://doi.org/10.1016/j.isprsjprs.2018.04.009.

WUDAPT (World Urban Database and Access Portal Tools). Available at: http://www.wudapt.org (last accessed: 15 Oct 2021)

Yang, X., Yao, L., Jin, T., Peng, L.L.H., Jiang, Z., Hu, Z. & Ye Y. (2018). Assessing the thermal behavior of different local climate zones in the Nanjing metropolis, China. *Building and Environment*, 137, 171–184. https://doi.org/10.1016/j.buildenv.2018.04.009

Yang, C., Yan, F. & Zhang, S. (2020). Comparison of land surface and air temperatures for quantifying summer and winter urban heat island in a snow climate city. *Journal of Environment Management*, 265, 110563. https://doi.org/10.1016/j.jenvman.2020.110563

Zhou, B., Rybski, D. & Kropp, J.P. (2013). On the statistics of urban heat island intensity. *Geophysical Research Letters*, 40, 5486–5491. https://doi.org/10.1002/2013GL057320

Zhu, W., Lü, A. & Jia, S. (2013). Estimation of daily maximum and minimum air temperature using MODIS land surface temperature products. *Remote Sensing of Environment*, 130, 62–73. https://doi.org/10.1016/j.rse.2012.10.034